energies

MDPI

Article

Sensorless Model Predictive Control of Permanent Magnet Synchronous Motors Using an Unscented Kalman Filter

Dariusz Janiszewski

Institute of Robotics and Machine Intelligence, Poznan University of Technology, 60965 Poznan, Poland; dariusz.janiszewski@put.poznan.pl

Abstract: This paper deals with the application of the *Model Predictive Control* (*MPC*) algorithm to the sensorless control of a *Permanent Magnet Synchronous Motor* (PMSM). The proposed estimation strategy, based on the *unscented Kalman filter* (*UKF*), uses only the measurement of the motor current for the online estimation of speed, rotor position and load torque. Information about the system state is fed into the *MPC* algorithm. The results verify the effectiveness and applicability of the proposed sensorless control technique. To demonstrate its real-world applicability, implementation in low-speed direct drive astronomy telescope mount systems is investigated. The outcomes of the implementation are thoroughly examined, leading to insightful conclusions drawn from the observed results. Through rigorous theoretical analysis and extensive simulation studies, this paper establishes a solid foundation for the proposed sensorless control technique. The results obtained from simulation studies and real-world applications underscore the efficacy and versatility of the proposed approach, offering valuable insights for the advancement of sensorless control strategies in motor applications. The main aim of this work is to demonstrate and validate the practical feasibility of combining two complex techniques, establishing that such an integration is not only possible but also effective in achieving the desired objectives.

Keywords: motion control; variable-speed drives; automatic control; predictive control; sensorless control; observers; Kalman filters; unscented Kalman filter; system modeling

Citation: Janiszewski, D. Sensorless Model Predictive Control of Permanent Magnet Synchronous Motors Using an Unscented Kalman Filter. *Energies* **2024**, *17*, 2387. https://doi.org/10.3390/en17102387

Academic Editors: Emmanuel Delaleau, Jean-Matthieu Bourgeot and Ahmed Abu-Siada

Received: 11 February 2024
Revised: 21 April 2024
Accepted: 1 May 2024
Published: 16 May 2024

1. Introduction

Permanent Magnet Synchronous Motor (PMSM) drives find extensive use in industrial processes owing to their inherently high torque-to-inertia ratio facilitated by their high flux density, compact size, and enhanced dynamic performance, making them ideal for applications where precision, responsiveness, and efficiency are paramount [1–4]. Discussions often revolve around enhancing the accuracy, stability, and robustness of their control methodologies. A widely used industrial control method, such as *field-oriented control* of PMSMs, heavily relies on an accurate rotor position [2]. However, the requirement for high-precision sensors comes at a cost, often requiring enclosed housing, which limits their applicability in specialized environments. In demanding conditions involving severe pressure, humidity, temperature, and vibration, traditional mechanical encoders prove inadequate [5,6]. Systems called *sensorless* systems present a potential solution by eliminating the necessity for mechanical sensors. This becomes particularly crucial during safety operations following sensor failure, especially in inaccessible environments [5]. Consequently, significant attention has been directed towards developing sensorless drives, utilizing the inherent behavior of PMSMs as a kind of virtual position sensor. In general, the advantages of these drive systems encompass potentially reduced drive costs, fewer integrated parts, a smaller size, a heightened reliability, and easier maintenance. However, their drawbacks primarily include a low load capacity, a limited speed accuracy, and instability in generating low-speed ranges [4,7].

In recent years, considerable research has focused on flux and shaft position estimation methods for drive systems in both induction motors and PMSMs, broadly categorized into two groups: those based on physical phenomena and those based on algorithmic methods, called observers. The exploration of these estimation methods reflects the growing emphasis on advancing motor control technologies, with a particular interest in developing robust and accurate techniques that leverage the understanding of physical motor behavior as well as sophisticated algorithmic approaches to ensure optimal performance and reliability in diverse industrial applications. Reference [8] outlines a primary method based on the physical non-linear behavior of magnetic circuits in induction motors. Additionally, the injection of high-frequency signals to emulate similar properties has also been applied [3,9]. The second major group involves algorithmic methods. The electromagnetic force (EMF) estimator has been extensively used to acquire speed and position information, as seen in [4,10,11]. Other proposed computational methods, such as those based on the basic sliding mode observer, are developed in [12,13]. Observers based on the Kalman filter (KF) [14] also find applications. For non-linear systems like PMSMs, extended Kalman filter (EKF)-based observers are prevalent [4,15–17]. However, due to the inherent unreliability and inaccuracy of the EKF for analytically undifferentiable non-linear circuits, an alternative approach using unscented transformations has emerged [18]. The unscented Kalman filter (UKF) stands out as an advanced filtering technique that significantly mitigates non-linearity issues associated with Gaussian noise and truncation errors, positioning itself as a viable and advantageous replacement for the extended Kalman filter (EKF). By employing a deterministic sampling approach, the UKF excels in capturing the true statistical characteristics of the underlying non-linear system dynamics [19,20]. This distinctive feature allows the UKF to outperform the EKF, especially in scenarios where the traditional filter may struggle with inaccuracies due to linearization, providing a more robust and accurate solution for state estimation in various engineering applications [4,21,22]. For certain complex non-linear systems, the resulting UKF more accurately estimates the true mean and covariance [23] in the scope of fast computations [24].

Model Predictive Control (MPC) is an advanced method in complex process control, frequently applied in chemical, pharmaceutical, petrochemical, and vehicle dynamics control systems. Its widespread adoption is attributed to its ability to optimize control inputs over a finite time horizon, considering the dynamic nature of the system and constraints imposed on the control variables. This forward-looking characteristic enables MPC to anticipate future system behavior and make proactive adjustments, making it particularly well suited for processes with intricate dynamics and stringent operational requirements [25–27]. The effectiveness of MPC lies not only in its ability to address complex control challenges but also in its integration with real-time optimization; its computational complexity and time demands limit applications to slower control cycle steps. MPC operates on an iterative control concept, leveraging a system model to predict future states within finite horizons, considering constraints and dynamic behaviors, requiring knowledge of the full system state—either measured or estimated. Notably, it has found successful applications in electromechanical systems in [28–30] and robotics in [31]. A neat and noteworthy summary of the possibilities of using MPC in motor control is presented in [30]. The recent literature [32] introduces MPC solutions for electric drive control, including current control in induction machines [16,33,34] and even in the domain of brushless DC motors with separate speed and current control [35]. Cascade MPC is commonly employed for speed control, enabling torque limitation to the maximum value while ensuring an optimal dynamic performance [32,34]. The solutions proposed in [36] and [37] advocate using the EKF as a state observer with a full state vector for MPC. Based on the comprehensive review of the literature presented in this article, it is evident that no comparable solutions or approaches have been documented or identified. A notable aspect worth highlighting is its implementation in a solution that closely resembles an industrial environment, contributing to its practical applicability and relevance to real-world scenarios.

Building upon the insights gained from previous authors' experience in sensorless control with PID controllers [4,38,39], the current research endeavors to elevate the precision of control systems through the integration of Model Predictive Control (MPC) for sensorless control of Permanent Magnet Synchronous Motors (PMSMs). A significant focus of this research lies in leveraging the state estimates obtained through the unscented Kalman filter (UKF) in conjunction with MPC. The seamless fusion of UKF-derived state information with the predictive capabilities of MPC holds promise for achieving a higher degree of accuracy in PMSM control.

This article covers the fundamental components of this research, including problem identification, a proposed solution supported by the literature, the theoretical framework, simulations, and a practical demonstration in a lab setting. This paper is divided into four sections: Following the introduction, the second section provides a detailed description of the considered control scheme, encompassing a basic mathematical model of the system, the fundamentals of the unscented Kalman filter, and Model Predictive Control, as well as a method for mutual exploitation. In the third section, the results, taking into account quality, are presented in two distinct steps: simulations and laboratory verification. Exemplary figures illustrating the operation of the proposed sensorless control structure are included. The document is then concluded in the final section.

2. Methods

The proposed cascade MPC is often used for speed control, which allows us to limit the torque (currents) to the maximum admissible value while providing optimal dynamic performance [32]. The opposite approach consists of introducing full Model Predictive Control. Controlled values are estimated by the unscented Kalman filter.

2.1. Proposed Sensorless Control Scheme

A block diagram of the proposed sensorless scheme is shown in Figure 1. Signals for the UKF, like stator currents i_a, i_b, i_c (measured by sensors) translated into i_α, i_β and desired voltages u_α, u_β, are defined as desired by the MPC scheme. For the values of natural output (currents, speed and position), only the desired speed ω_r^* was chosen. The presented algorithm requires knowledge of the state variables $\underline{\hat{x}}$.

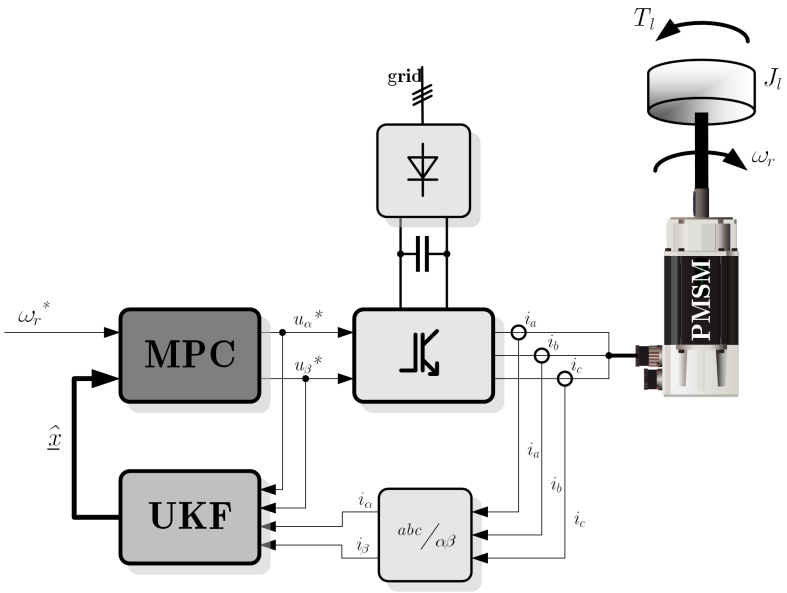

Figure 1. Control system scheme.

The effectiveness of the proposed drive system has been verified in the scheme in Figure 1.

2.2. Mathematical Model of a PMSM for MPC and the UKF

The process model plays a decisive role in the controller. In order to predict the future behavior of a process, we must have a model of how the process behaves. A model is also necessary for the expected signal estimation via the unscented Kalman filter. The chosen model must be able to capture the process dynamics to predict the future outputs based on estimated states with precision.

The mathematical model of the PMSM has three main parts: the electrical network, electromechanical torque production and the mechanical subsystem [40]. The stator of the PMSM and the induction motor are similar. The rotor consists of permanent magnets (modern rare-earth magnets with a high strength).

During investigations, some simplified assumptions are made: saturation is negligible, the inducted electromagnetic force is sinusoidal, eddy currents and hysteresis losses are negligible, there are no dynamical dependencies in the air gap, and there is no rotor cage. Under these assumptions, the rotor-oriented dq electrical network equations of the PMSM can be described as:

$$u_d = R_s i_d + L_d \frac{di_d}{dt} - p\omega_r L_q i_q \,, \tag{1}$$

$$u_q = R_s i_q + L_q \frac{di_q}{dt} + p\omega_r L_d i_d + p\omega_r \Psi_m \,. \tag{2}$$

where u_d, u_q are dq axis voltages; i_d, i_q are dq axis currents; L_d, L_q are dq axis inductances; R_s is stator resistance; and Ψ_m is the magnetic flux produced by permanent magnets placed on the rotor.

The value of the produced electromagnetic torque is given by the following equation:

$$T_e = \frac{3}{2} \cdot p\left[\Psi_m - \left(L_q - L_d\right) i_d\right] \cdot i_q \,, \tag{3}$$

where p is the number of pole pairs, and the fraction $\frac{3}{2}$ stems from frame conversion, i.e., perpendicular stator $\alpha\beta$ over rotor dq.

The drive dynamics can be described as:

$$T_e - T_{load} = J \frac{d\omega_r}{dt}, \tag{4}$$

where T_{load} is the load torque and J is the summary moment of inertia of the kinematic chain.

Based on (3) and (4), the movement equation is:

$$\frac{d\omega_r}{dt} = \frac{p}{J}\left[\frac{3}{2}\left(\Psi_m - \left(L_q - L_d\right) i_d\right) \cdot i_q\right] - \frac{T_e}{J} \,. \tag{5}$$

The otor position γ can be described by the derivative equation of the rotational speed:

$$\frac{d\gamma}{dt} = p \cdot \omega_r \,. \tag{6}$$

Drawing inspiration from the concept of the dual Kalman filter described in reference [41], one or more parameters can be treated as estimation values. The load torque T_l is considered as such a *virtual* parameter within the proposed framework, enabling its observation and estimation. This approach opens avenues for dynamic adaptation and refinement [4,39,42], as in this case, the load torque is not merely an unknown disturbance but is dynamically observed and estimated, enhancing the adaptability of the control system in response to varying operational conditions. The true assumption that the load torque T_l is invariable in a narrow interval holds:

$$\frac{d}{dt} T_l \approx 0 \,. \tag{7}$$

The discrete state space is obtained from the continuous state space by discretization of coefficient matrices with the first-order *backward Euler method* with step time T_s. The step time was chosen to be far beyond the Nyquist frequency based on system poles, and is equal to the *PWM* frequency of the power electronics part. This is a hardware-implementation-oriented assumption. The state-space model can be described as a classical discrete state-space model:

$$\underline{\hat{x}}_k = \mathbf{F}_k(\underline{\hat{x}}_{k-1})\underline{\hat{x}}_{k-1} + \mathbf{B}_k(\underline{\hat{x}}_{k-1})\underline{u}_k\,, \tag{8}$$

$$\underline{z}_k = \mathbf{H}_k(\underline{\hat{x}}_k)\underline{\hat{x}}_k\,, \tag{9}$$

For the synthesis of the unscented Kalman filter, state vector $\hat{x}$ was chosen:

$$\underline{\hat{x}} = \left[\hat{i}_d\ \hat{i}_q\ \hat{\omega}_r\ \hat{\gamma}\ \hat{T}_l\right]^T, \tag{10}$$

with all natural state variables and estimated load torque $\hat{T}_l$. Considering the above, the system matrix $\mathbf{F}_k$ has the form:

$$\mathbf{F}_k(\underline{\hat{x}}_k) = \begin{bmatrix} 1 - T_s \cdot \frac{R_s}{L_d} & T_s \cdot \omega_r \frac{L_q}{L_d} & 0 & 0 & 0 \\ -T_s \cdot \omega_r \frac{L_d}{L_q} & 1 - T_s \cdot \frac{R_s}{L_q} & -T_s \cdot \frac{\Psi_m}{L_q} & 0 & 0 \\ 0 & T_1 & 0 & 0 & -T_s \cdot \frac{1}{J} \\ 0 & 0 & T_s & 1 & 0 \\ 0 & 0 & 0 & 0 & 1 \end{bmatrix}, \tag{11}$$

where

$$T_1 = T_s \cdot \frac{3}{2}\frac{p}{J}\Big[\Psi_f - (L_q - L_d)i_d\Big].$$

The output matrix $\mathbf{H}_k$ is a rotating matrix via the Clark/Parck transformation:

$$\mathbf{H}_k(\underline{\hat{x}}_k) = \begin{bmatrix} \cos\gamma & -\sin\gamma & 0 & 0 & 0 \\ \sin\gamma & \cos\gamma & 0 & 0 & 0 \end{bmatrix}, \tag{12}$$

and matrix $\mathbf{B}_k$:

$$\mathbf{B}_k(\underline{\hat{x}}_k) = \begin{bmatrix} T_s \cdot \frac{1}{L_d}\cos\gamma & T_s \cdot \frac{1}{L_d}\sin\gamma \\ -T_s \cdot \frac{1}{L_q}\sin\gamma & T_s \cdot \frac{1}{L_q}\cos\gamma \\ 0 & 0 \\ 0 & 0 \\ 0 & 0 \end{bmatrix}. \tag{13}$$

The state matrices are simplified. The load torque T_l is treated as a known disturbance. The appearance of the model of decoupled dq axes determines the method of control.

As evident from the proposed model analysis above, the system under consideration is non-linear, and this non-linearity is apparent in the state, input, and output matrices. The presented non-linear system involves matrices $\mathbf{H}_k$ described as (12), $\mathbf{B}_k$ as (13), and $\mathbf{F}_k$ in the form of (11), all of which are non-linear. Specifically, $\mathbf{H}_k$ and $\mathbf{B}_k$ incorporate trigonometric functions, reflecting a dependency on state variables associated with two-axis rotation ($\alpha\beta$, dq frames), while $\mathbf{F}_k$ includes non-neglected state multiplications.

An issue may arise in accurately determining the current state based on both current and historical inputs. Additionally, in the presence of high non-linearities, the space of variable occurrences becomes disrupted, leading to non-linear variances for state $\mathbf{P}_x$ and outputs $\mathbf{P}_y$, which characterizes the accuracy of the modeling process. This disruption further complicates the characterization of variables in a non-linear space.

2.3. Unscented Kalman Filter

The primary challenge in estimating non-linear systems lies in determining the non-linear function of the state and output, as discussed by [19,43]. Additionally, addressing non-linearities in the probability distribution further complicates the task [18]. It seems that the non-linear transformation and the inclusion of Jacobians in the extended Kalman filter (EKF) may not accurately determine real covariances [18]. The unscented Kalman filter (UKF) emerges as an advancement over prior algorithms, presenting a novel solution to the estimation theory problem based on unscented transformations [18,19]. Unlike the EKF, the UKF simplifies the definition and approximation of the Gaussian distribution associated with each state vector variable, as opposed to relying on the approximation of non-linear function transformations [19]. Moreover, the EKF streamlines the algorithm by eliminating the need to calculate Jacobians at each working point. This streamlining is grounded in two key assumptions. Firstly, it involves determining the non-linear transformation of the function at work, rather than across the entire range of the probability density distribution function. Secondly, it revolves around identifying working points where this density aligns with the actual decomposition of the non-linear system. This filter, like its classical form, is based on two cycles: *prediction* and *correction* [14].

The prediction of the UKF can be used independently from the UKF update, in combination with a linear update. In this case, however, the estimation state vector of the value of disturbances is extended. Such a procedure makes it possible to estimate the state vector and its environment (with disturbances).

Based on [19], the defined augmented estimation vector $\underline{x}^a_{k-1|k-1}$ can be defined as:

$$\underline{x}^a_{k-1|k-1} = [\underline{\hat{x}}^T_{k-1|k-1} \quad E\langle \underline{w}^T_k \rangle \quad E\langle \underline{v}^T_k \rangle \,]^T \tag{14}$$

which consists of state vector $\hat{x}_k$ and expected noise terms w_k and v_k, with the definition of each covariance given as:

$$\mathbf{P}^a_{k-1|k-1} = \begin{bmatrix} \mathbf{P}_{k-1|k-1} & 0 & 0 \\ 0 & \mathbf{Q}_k & 0 \\ 0 & 0 & \mathbf{R}_k \end{bmatrix}. \tag{15}$$

where $\mathbf{Q}_k$ is defined as the covariance of process noise and $\mathbf{R}_k$ is the covariance of observation (measurement) noise.

An important set of $2L+1$ sigma points, $\chi_{k-1|k-1}$, is derived from the augmented state and covariances, where L is the dimension of the augmented state:

$$\chi^0_{k-1|k-1} = \underline{x}^a_{k-1|k-1}, \tag{16}$$

$$\chi^i_{k-1|k-1} = \underline{x}^a_{k-1|k-1} + \left(\sqrt{(L+\lambda)\mathbf{P}^a_{k-1|k-1}}\right)_i, \tag{17}$$

$$\text{for } i = 1..L,$$

$$\chi^i_{k-1|k-1} = \underline{x}^a_{k-1|k-1} - \left(\sqrt{(L+\lambda)\mathbf{P}^a_{k-1|k-1}}\right)_{i-L}, \tag{18}$$

$$\text{for } i = L+1, \ldots 2L,$$

The matrix square root $\left(\sqrt{(L+\lambda)\mathbf{P}_k}\right)$ should be calculated using numerically efficient and stable methods such as the *Cholesky decomposition*, where the $(L+\lambda)$ coefficient was chosen based on [44].

The sigma points $\chi^i_{k|k-1}$ are propagated through the state-space transition function:

$$\chi^i_{k|k-1} = \mathbf{F}_k \chi^i_{k-1|k-1} + \mathbf{B}_k \underline{u}_k, \quad i = 0..2L. \tag{19}$$

The weighted sigma points $\chi^i_{k|k-1}$ are recombined to produce the predicted state $\underline{\hat{x}}_{k|k-1}$ and covariance $\mathbf{P}_{k|k-1}$:

$$\underline{\hat{x}}_{k|k-1} = \sum_{i=0}^{2L} W_s^i \chi^i_{k|k-1}\,, \tag{20}$$

$$\mathbf{P}_{k|k-1} = \sum_{i=0}^{2L} W_c^i \,[\chi^i_{k|k-1} - \underline{\hat{x}}_{k|k-1}][\chi^i_{k|k-1} - \underline{\hat{x}}_{k|k-1}]^T\,, \tag{21}$$

where the weights W_s and W_c for the state and covariance [44] are given by:

$$W_s^0 = \tfrac{\lambda}{L+\lambda}\,, W_c^0 = \tfrac{\lambda}{L+\lambda} + (1 - \alpha^2 + \beta)\,, \tag{22}$$

$$W_s^i = W_c^i = \tfrac{1}{2(L+\lambda)}\,, \tag{23}$$

with:

$$\lambda = \alpha^2(L + \kappa) \tag{24}$$

where α, β, κ are noise distribution parameters, and λ is chosen arbitrarily. Making informed choices during filter tuning, as emphasized in [19], proves beneficial. For most applications where disturbances adhere to Gaussian noise assumptions, typical values for α, β, and κ are conventionally set at 10^{-3}, 2, and 0, respectively. Introducing the κ factor provides an opportunity to incorporate an additional degree of freedom during tuning, particularly when *non-Gaussian* disturbance occurrences.

During *correction*, the sigma points $\chi^i_{k|k-1}$ are projected through the observation function $\mathbf{H}_k$:

$$\mathrm{Y}^i_k = \mathbf{H}_k \chi^i_{k|k-1}\,, \quad i = 0..2L\,. \tag{25}$$

Based on weights W_s^i and W_c^i from Equation (23) and the observation matrix Y^i_k, it is possible to obtain the following output signal:

$$\underline{\hat{z}}_k = \sum_{i=0}^{2L} W_s^i \mathrm{Y}^i_k\,, \tag{26}$$

and also the output covariance:

$$\mathbf{P}_{z_k z_k} = \sum_{i=0}^{2L} W_c^i \,[\mathrm{Y}^i_k - \underline{\hat{z}}_k][\mathrm{Y}^i_k - \underline{\hat{z}}_k]^T\,. \tag{27}$$

The solution of the classical form of the Kalman filter is adapted in the UKF. Correction $\mathbf{K}_k$ depends directly on state covariances $\mathbf{P}_{k|k-1}$ and the innovation of system covariances $\mathbf{S}_k$, so it is similar to (27):

$$\mathbf{K}_k = \mathbf{P}_{x_k z_k} \mathbf{P}^{-1}_{z_k z_k}\,, \tag{28}$$

where $\mathbf{P}_{x_k z_k}$ can be described as:

$$\mathbf{P}_{x_k z_k} = \sum_{i=0}^{2L} W_c^i \,[\chi^i_{k|k-1} - \underline{\hat{x}}_{k|k-1}][\mathrm{Y}^i_k - \underline{\hat{z}}_k]^T\,. \tag{29}$$

As in the classical Kalman filter, the residuum is output as:

$$\underline{\tilde{y}}_k = \underline{z}_k - h(\underline{\hat{x}}_{k|k-1})\,. \tag{30}$$

Correction of state is achieved via:

$$\underline{\hat{x}}_{k|k} = \underline{\hat{x}}_{k|k-1} + \mathbf{K}_k(\underline{z}_k - \underline{\hat{z}}_k)\,. \tag{31}$$

The adjusted covariance matrix $\mathbf{P}_{k|k}$ is a prediction of $\mathbf{P}_{k|k-1}$, corrected by weighted values:

$$\mathbf{P}_{k|k} = \mathbf{P}_{k|k-1} - \mathbf{K}_k \mathbf{P}_{z_k z_k} \mathbf{K}_k^T . \tag{32}$$

The algorithm operates in a recursive manner, utilizing data from the current step as input for the subsequent step.

2.4. Model Predictive Control

Model Predictive Control is an advanced control scheme where the control signal is obtained by solving an open-loop optimal multi-variable control problem across a predefined predictive horizon. A method commonly referred to as *Receding Horizon Control* is used, as discussed in [27]. The objective of this approach is to optimize and generate an optimal control sequence, considering predefined cost criteria and adhering to specified control and system constraints.

Philosophically, Model Predictive Control (MPC) reflects human decision-making processes by autonomously selecting control actions that are projected to produce the most favorable predicted outcomes or outputs within a finite time. This parallels the cognitive process in which humans anticipate future consequences and adjust their actions accordingly, emphasizing the proactive and forward-thinking nature of both MPC and human decision-making. In practical terms, it imposes constraints on planning, decision-making, and resource utilization, necessitating efficient utilization within the specified timeframe. Understanding the finite nature of the horizon is crucial for managing expectations, setting goals, and implementing strategies effectively. This approach aligns with the human tendency to consider future consequences when making decisions. In normal applications, a singular MPC-based controller assumes the pivotal role of overseeing the entire system, possessing a comprehensive understanding of system behavior and all computed control signals. This centralized control perspective allows MPC to proactively shape the system's trajectory, adjusting inputs in real time to optimize performance and adhere to defined objectives. The dynamic and anticipatory nature of MPC underscores its similarity with human decision-making processes, emphasizing the importance of foresight and adaptability in achieving optimal outcomes in complex control scenarios.

2.4.1. Principle

One notable advantage of predictive control mentioned above lies in its inherent simplicity and intuitive concepts. The essence of Model Predictive Control (MPC) is rooted in the straightforward idea that the controller must anticipate the future behavior of the system. At the heart of MPC lies the model of the system, as elucidated above. The efficacy of the control law is intricately tied to the accuracy of predictions, making the model a pivotal component in steering the system toward optimal performance. By leveraging this predictive capability, MPC enables a proactive and adaptive control strategy, making it a valuable tool in scenarios where anticipating and responding to future states is crucial for achieving desired control outcomes.

In the literature, MPC is formulated in the state-space approach. Let the model of the plant to be controlled be described by the linear discrete-time state-space equations:

$$\underline{x}_{k+1} = \mathbf{A}\underline{x}_k + \mathbf{B}\underline{u}_k \tag{33}$$

$$\underline{y}_k = \mathbf{C}\underline{x}_k + \mathbf{D}\underline{u}_k \tag{34}$$

where:

$$\underline{x} \in \mathbf{X} \in \mathbb{R}^n,\ \underline{y} \in \mathbf{Y} \in \mathbb{R}^p,\ \underline{u} \in \mathbf{U} \in \mathbb{R}^m, \tag{35}$$

are the vectors of state, output and input, respectively. The cost function J_N that has to be minimized in the receding horizon N generally takes the quadratic form:

$$J_N = \sum_{j=k}^{k+N-1} \left(\underline{x}_j^T Q \underline{x}_j + \underline{u}_j^T R \underline{u}_j \right) \tag{36}$$

where Q and R are particular scaling parameters of sensitivity of the minimization of internal behavior x_j (represented by the Q factor) and external u_j behavior (represented by the$R$ factor).

When we assume an N-step prediction, the system output behavior can be determined in the following N steps:

$$\underbrace{\begin{bmatrix} \underline{y}_0 \\ \underline{y}_1 \\ \vdots \\ \underline{y}_{N-1} \end{bmatrix}}_{\mathbf{y}} = \underbrace{\begin{bmatrix} \mathbf{C} \\ \mathbf{CA} \\ \vdots \\ \mathbf{CA}^{N-1} \end{bmatrix}}_{\mathbf{O}_N} \underline{x}_0 + \underbrace{\begin{bmatrix} \mathbf{H}_0 & 0 & 0 & \cdots & 0 \\ \mathbf{H}_1 & \mathbf{H}_0 & 0 & \cdots & 0 \\ \mathbf{H}_2 & \mathbf{H}_1 & \mathbf{H}_0 & \cdots & 0 \\ \vdots & \vdots & \vdots & \ddots & \vdots \\ \mathbf{H}_{N-1} & \mathbf{H}_{N-2} & \cdots & \cdots & \mathbf{H}_0 \end{bmatrix}}_{\mathbf{H}_N} \underbrace{\begin{bmatrix} \underline{u}_0 \\ \underline{u}_1 \\ \vdots \\ \underline{u}_{N-1} \end{bmatrix}}_{\mathbf{u}} \tag{37}$$

written most simply as:

$$\mathbf{y} = \mathbf{O}_N \underline{x}_0 + \mathbf{H}_N \underline{u}_0 \,, \tag{38}$$

where:

$$\mathbf{O}_0 = \mathbf{C},\ \mathbf{O}_k = \mathbf{CA}^k,\ k = 1, 2, \cdots, N-1 \tag{39}$$

$$\mathbf{H}_0 = \mathbf{D},\ \mathbf{H}_k = \mathbf{CA}^{k-1}\mathbf{B},\ k = 1, 2, \cdots, N-1 \tag{40}$$

Based on the above and the definition of optimization cost in (36), these can be compared with the desired state of the system:

$$J_N = \sum_{p=0}^{N-1} \left(\underline{w}_p - \underline{y}_p \right)^T \left(\underline{w}_p - \underline{y}_p \right) = \left[(\mathbf{w} - \mathbf{y})^T (\mathbf{w} - \mathbf{y}) \right]_N . \tag{41}$$

The optimizer is a crucial part of the strategy, as it provides the control. The combination of (36) and (41) can be solved by the *quadratic programming (QP)* problem as:

$$J_N = \mathbf{u}^T \mathbf{H}_N^T \mathbf{H}_N \mathbf{u} + 2 \left(\underline{x}_0^T \mathbf{O}_N \mathbf{H}_N - \mathbf{w}^T \mathbf{H}_N \right) \tag{42}$$

to minimize the value of the control signal $\mathbf{u}$ in each future predicted state N. The reference speed signal is introduced into the $\mathbf{w}$ vector.

Since the problem depends on the current state $\underline{x}$ and the importance matrix $\mathbf{Q}$ introduced into (42), it looks like:

$$J_N = \mathbf{u}^T \mathbf{H}_N^T \mathbf{Q} \mathbf{H}_N \mathbf{u} + 2 \left(\underline{x}_0^T \mathbf{O}_N \mathbf{H}_N - \mathbf{w}^T \mathbf{H}_N \right) . \tag{43}$$

The solution of the MPC problem requires the online solution of a *QP* at each time step.

2.4.2. Constraints

Based on finding the min of cost function (42), which has the form:

$$\min J_N \rightarrow \min_{\mathbf{u}} \frac{1}{2} \mathbf{u}^T \mathbf{H} \mathbf{u} + \mathbf{f} \mathbf{u} \,, \tag{44}$$

it is possible to introduce some constraints which state that:

$$\mathbf{A} \mathbf{u} \leq \mathbf{b} \,. \tag{45}$$

Considering the maximum possible supply voltage:

$$\underline{u}_{min} \leq \underline{u}_k \leq \underline{u}_{max} \tag{46}$$

and the suspected predicted state constraints:

$$\underline{x}_{min} \leq \underline{x}_k \leq \underline{x}_{max}\,, \tag{47}$$

QP yields optimized results according to (44).

This paper focuses specifically on the *dq* axis current (i_d and i_q) limitation and maximum supply voltage (u_α and u_β). Other limitations seem not to apply here.

The presented optimization approach can now be identified and simplified to address the *QP* problem with linear inequality constraints [45]. While the optimization problem exhibits the desirable property of convexity, the presence of constraints complicates the situation. Despite the convex nature of the problem, these constraints hinder the derivation of a straightforward, explicit solution formula. Regarding performance, there are a few methods for solving the *QP problem*, like *interior-point*, *active set*, and *sequential qp* methods, which possess unique characteristics when applied to MPC. In this work, the decision was made to utilize the *active set* algorithm with iterative state values [46].

3. Results

To achieve optimal performance and efficiency in control systems, diverse control techniques are employed to regulate parameters such as the speed, torque, and rotor position. This investigation has presented a comprehensive categorization of speed control methods. Among these methods, the vector control technique emerges as a prominent approach for governing the speed of PMSMs. Furthermore, the vector control technique is commonly known as *field-oriented control* (FOC) [2]. Model Predictive Control is one of the most practical advanced control techniques in industrial applications.

However, the MPC approach requires the selection of the control matrix **Q** for the optimization system. Taking into account the entire control vector:

$$\underline{x} = \begin{bmatrix} i_d & i_q & \omega_r & \gamma \end{bmatrix} \tag{48}$$

based on the proposed model with states defined as (10), **Q** can be a specified internal importance factor:

$$\mathbf{Q} = diag\{\tilde{i}_d \; \tilde{i}_q \; \tilde{\omega}_r \; \tilde{\gamma}\}\,. \tag{49}$$

To align with the speed vector control scheme, prioritizing the speed variable ω_r is imperative, making its coefficient $\tilde{\omega}_r$ pivotal and substantial. Given that vector control employs cascade control alongside current controllers, ensuring non-zero values for $\tilde{i}_d$ and $\tilde{i}_q$ is essential. In the scenario presented, where position control is not a consideration, the associated value $\tilde{\gamma}$ should be set to zero.

An essential component of the MPC system, assuming a vector of control state variables $\underline{x}$ like (48), is the definition of an object in state-space form (**A**, **B**, **C**, **D**) as the relations (33) and (34). Considering the model of an object described in Section 2.2, with state matrices described by (11), (12) and (13), **A**, **B**, **C**, **D** take the form:

$$\mathbf{A} = \begin{bmatrix} 1 - T_s \cdot \frac{R_s}{L_d} & T_s \cdot \omega_r \frac{L_q}{L_d} & 0 & 0 \\ -T_s \cdot \omega_r \frac{L_d}{L_q} & 1 - T_s \cdot \frac{R_s}{L_q} & -T_s \cdot \frac{\Psi_m}{L_q} & 0 \\ 0 & T_1 & 0 & 0 \\ 0 & 0 & T_s & 1 \end{bmatrix}, \tag{50}$$

where:

$$T_1 = T_s \cdot \frac{3}{2}\frac{p}{J}\left[\Psi_f - (L_q - L_d) i_d\right],$$

$$\mathbf{B} = \begin{bmatrix} T_s \cdot \frac{1}{L_d} \cos\gamma & T_s \cdot \frac{1}{L_d} \sin\gamma \\ -T_s \cdot \frac{1}{L_q} \sin\gamma & T_s \cdot \frac{1}{L_q} \cos\gamma \\ 0 & 0 \\ 0 & 0 \end{bmatrix}. \tag{51}$$

$$\mathbf{C} = \begin{bmatrix} \cos\gamma & -\sin\gamma & 0 & 0 \\ \sin\gamma & \cos\gamma & 0 & 0 \end{bmatrix}, \tag{52}$$

$$\mathbf{D} = \begin{bmatrix} 0 & 0 \\ 0 & 0 \end{bmatrix}. \tag{53}$$

Regarding performance, there are a few methods for solving the *QP problem,* like *interior-point, active set, sequential qp* methods, which possess unique characteristics when applied to MPC. In this work, the decision was made to utilize the *active set* algorithm with iterative state values.

3.1. Preliminary Simulation Research

Evaluating control algorithms through simulations has emerged as a highly effective strategy for assessing the adequacy of motor controller designs. This approach not only provides a comprehensive understanding of the algorithm's performance but also significantly reduces the time and costs associated with the development process before transitioning to laboratory hardware testing. Simulations offer a controlled environment where various scenarios and operating conditions can be systematically examined. During this stage, a simulation model of a typical direct-drive environment was constructed. The core of simulations were performed using the *MATLAB* environment with the following toolboxes: *Control System, Optimalization* with set of *QP* problem solvers. As part of the verification process, a comparable scheme was employed, mirroring the setup used in the tests of the sensorless system with a *PID* controller as documented in [4,38]. The first element of the research was tuning at the appropriate observer level and selecting the parameters so that the estimation result is sufficiently close to that of another measurement method, assuming possible deviations.

During the utilization of the model, several simplifications were implemented. For instance, the mechanical component, including the intricate friction mechanism, was streamlined into a single-mass system with minimal friction. Additionally, the power electronics converter system, featuring a PWM modulator, was substituted with a unit delay and a conversion factor derived from the supply voltage. Similarly, the concurrent delay within the control system was replaced with a unit delay. A crucial aspect involves tuning the Kalman filter by selecting initial values for (15), such as $\mathbf{P}_{0|0}$, $\mathbf{Q}_0$, and $\mathbf{R}_0$. In this instance, the initial matrices were determined based on references [4,47], with their corresponding system parameters detailed in Table A1 (Appendix A), as:

$$\mathbf{Q}_0 = diag\left\{0.45 \cdot 10^{-3},\ 0.45 \cdot 10^{-3},\ 1.5 \cdot 10^{-8},\ 2.1 \cdot 10^{-11},\ 0.1\right\} \tag{54}$$

and

$$\mathbf{R}_0 = diag\left\{0.45 \cdot 10^{-3},\ 0.45 \cdot 10^{-3}\right\} \tag{55}$$

which correlate with system and output noises, with $\mathbf{P}_{0|0}$ defined as a zero starting point:

$$\mathbf{P}_{0|0} = \mathbf{0}\,, \tag{56}$$

which is assessed throughout the UKF algorithm computation.

The set-speed ω_r^* test was used for simulation tests, identical to subsequent laboratory tests as in Figure 2. The speed command has crucial elements, including the initialization of zero initial values, a sudden spike in the speed command, and an abrupt change in the direction of speed.

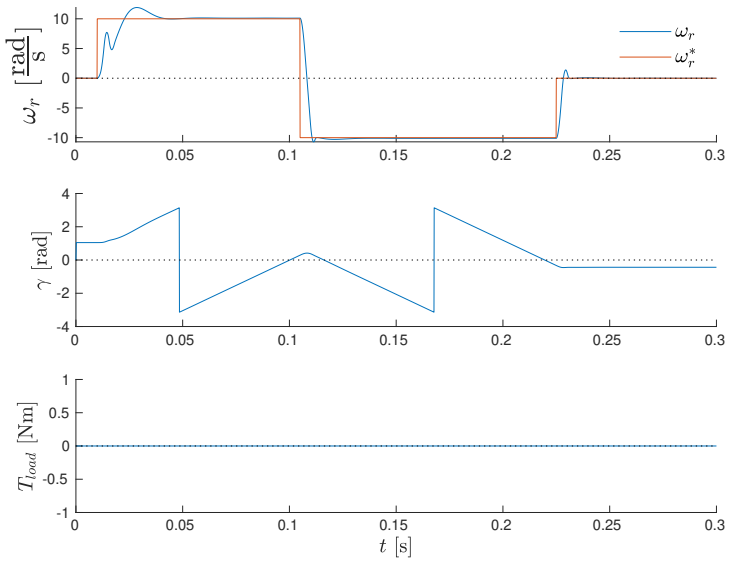

Figure 2. Speed ω_r, position γ and load torque T_{load} during desired speed change—simulation investigations.

During a series of simulations, it is worth comparing the entire group qualitatively and quantitatively. It was decided to use qualitative indicators regarding the stability of the closed control loop (**Stable**) and the ability to reach a constant desired signal ω_R^* in a finite time $t = 0.5\,\text{s}$ without static error (ω_r^* **reachable**). Measurable quality indexes like the *Integral Absolute Error* and *Integral Time Absolute Error* were defined as:

$$IAE_{full} = \int_{t_0}^{t_{end}} |\omega_r - \omega_r^*| dt \tag{57}$$

$$ITAE_{start} = \int_{t_0}^{t_{start}} t \cdot |\omega_r - \omega_r^*| dt \tag{58}$$

where the experiment starting time t_0 is 0 s, t_{end} is 0.3 s, and t_{start} was chosen as the longest acceptable settling time of desired speed during experiment, at 0.1 s.

Typical simulation results for $\mathbf{Q} = [1\ 1\ 30\ 0]$ with the best quality are presented in Figures 2 and 3, with a focus on showing two issues: the trends in mechanical and electrical quantities, respectively.

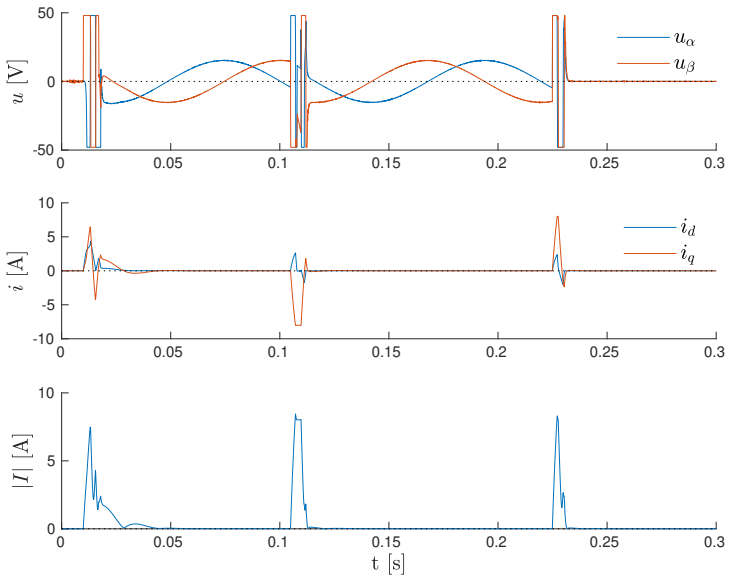

Figure 3. $\alpha\beta$ axis control voltages, dq axis current value, current modulus during desired speed change —simulation investigations.

Table 1 presents the mentioned indexes in relation to the tuning process by changing the **Q** vector.

Table 1. Influence of the tuning matrix **Q** on the control quality.

Horizon	Q	Stable	ω_r^* Reachable	IAE_{full}	$ITAE_{start}$
7	[1 1 1 0]	Y	N	0.760	0.815
7	[1 1 2 0]	Y	N	0.727	0.797
7	[1 1 5 0]	Y	N	0.438	0.580
7	[1 1 10 0]	Y	N	0.262	0.338
7	[1 1 20 0]	Y	Y	0.177	0.257
7	**[1 1 30 0]**	**Y**	**Y**	**0.147**	**0.226**
7	[1 1 50 0]	*limit of stab.*	Y	0.123	0.204
7	[1 1 55 0]	N	N	–	–
3	[1 1 30 0]	N	N	–	–
5	[1 1 30 0]	Y	Y	0.172	0.244
7	[1 1 30 0]	Y	Y	0.147	0.226
9	[1 1 30 0]	Y	Y	0.136	0.217

3.2. Laboratory Verification

After the numerous simulation studies presented above, an experimental verification of the proposed control method, following previous methods, was conducted. Implementation in real astronomy telescope mount systems was investigated [48]. The base axis of the laboratory stand, presented in Figure 4, consists of a surface-mounted magnet synchronous motor, supplied by a three-phase MOSFET power inverter controlled by a *Texas Instruments Sitara AM335x* and an *Altera FPGA Cyclone IV* board. The proposed control algorithm is divided into a few parts: hardware maintenance, estimation (UKF), and control (MPC). All matrix linear algebra operations were implemented using dlib++ libraries like dlib/matrix, dlib/vector and dlib/rectangle. The entire MPC algorithm was implemented based on **dlib/control** and dlib/optimization.

(**a**) (**b**)

Figure 4. The prototype astronomical mount with an 11″ telescope: (**a**) laboratory setup, (**b**) one-axis experimental setup with a variable moment of inertia.

The MPC algorithm that was developed was tested in extensive simulations under various conditions both prior to and during its implementation. The real results are only partly presented below to demonstrate its operation. The advantages of the sensorless UKF with a coordinated PI current and speed controllers were considered during the tuning

of the observer. From the collection of sets, one conditional example was chosen for the number of predicted states $N = 5$. Equation (42) was extended into:

$$J_N = \mathbf{u}^T \mathbf{H}_N^T \mathbf{Q} \mathbf{H}_N \mathbf{u} + 2\left(\underline{x}_0^T \mathbf{O}_N \mathbf{H}_N - \mathbf{w}^T \mathbf{H}_N\right) \tag{59}$$

which is:

$$\mathbf{Q} = diag\{1\ 1\ 30\ 0\}, \tag{60}$$

with a maximum related weight equal to 30 for a speed ω_r control surrounded by ones based on numerous simulation studies. Originally, the prediction horizon was set to $N = 7$, but after the first implementation, it turned out that the processor's computational efficiency was too low and this number was reduced to $N = 5$. The impact of this change was tested in simulation investigations and the values of quality factors were added to Table 1 above. An important point of this investigation under laboratory setup constraints setting the maximum value of the control signal was $|U| \leq 48$ V and the maximum value of currents (state vector $\underline{x}$ elements) was $|i_d| \leq 8$ A, $|i_q| \leq 8$ A in a circular shape.

The state observer based on the UKF was tuned similar to a classical coordinate system [22], with any special tuning. This proved to be an important indication of the possibility of using the estimated state $\underline{\hat{x}}$ as a control state $\underline{x}$.

The first part of this investigation was focused on controlling the system behavior via reference speed ω_r^* changes and the possibilities of obtaining the initial position γ after the algorithm was started.

Figure 5 shows the system's response to the rapid change in speed ω_r^*. Additional interesting signals (including actual control voltages $\underline{u}^*$) are presented in Figure 6.

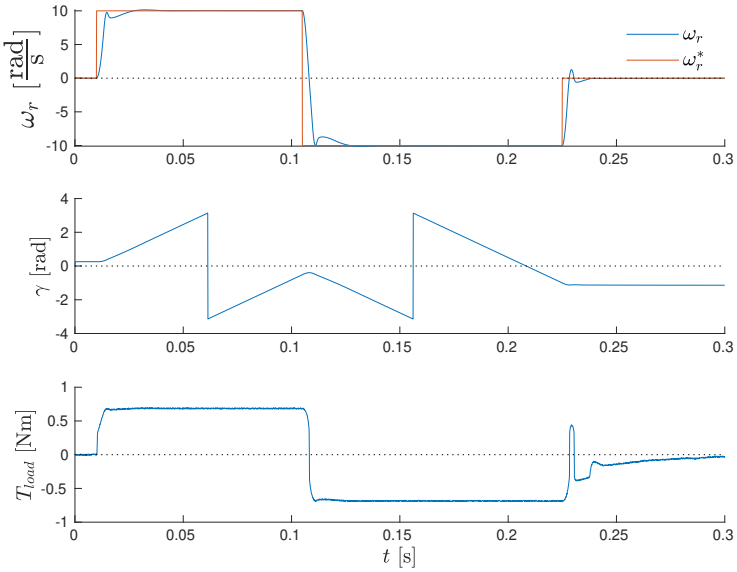

Figure 5. Speed ω_r, position γ and load torque T_{load} during the desired speed change.

An initial point $\hat{x}_0$ can be found by applying any voltage to the drive based on the first predictive step. The unscented Kalman filter in that form can determine the proper actual position of γ after a few steps. This process does not interfere with the MPC algorithm.

Additional investigations concern the external load torque disturbances and the kick type additional force. The properties are presented in Figure 7. A fast dynamic reaction can be observed but a steady-state error remains. The actual control voltages $\underline{u}^*$ and motor currents i_d, i_q with modulus I are presented in Figure 8.

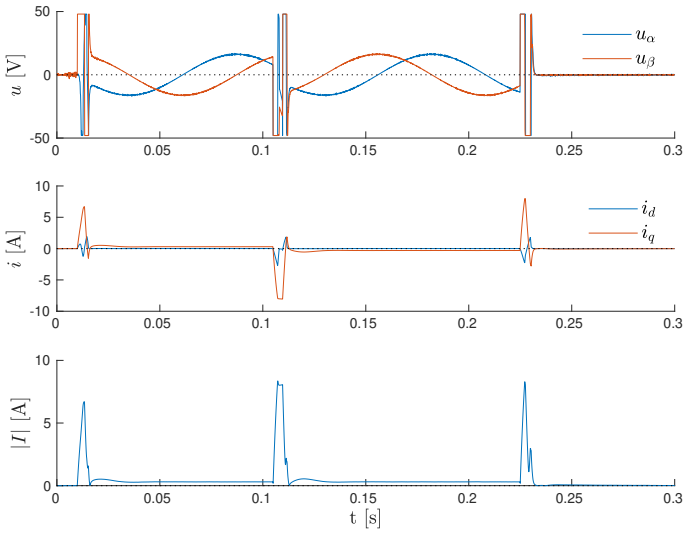

Figure 6. $\alpha\beta$ axis control voltages, dq axis current value, current modulus during the desired speed change.

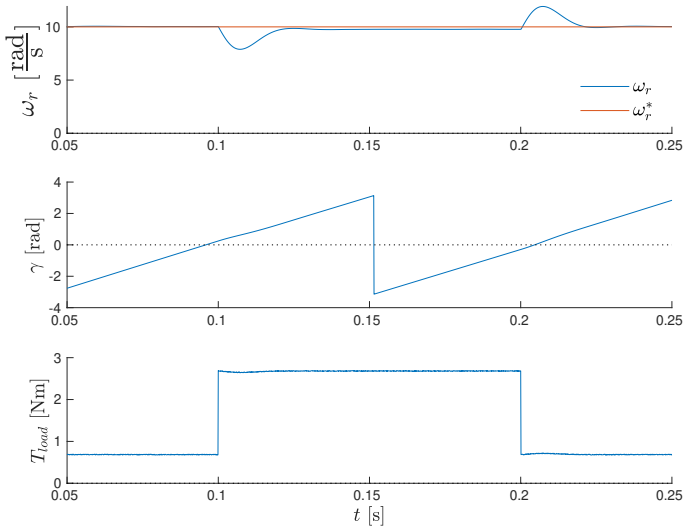

Figure 7. Speed ω_r, position γ and load torque T_l during load acting.

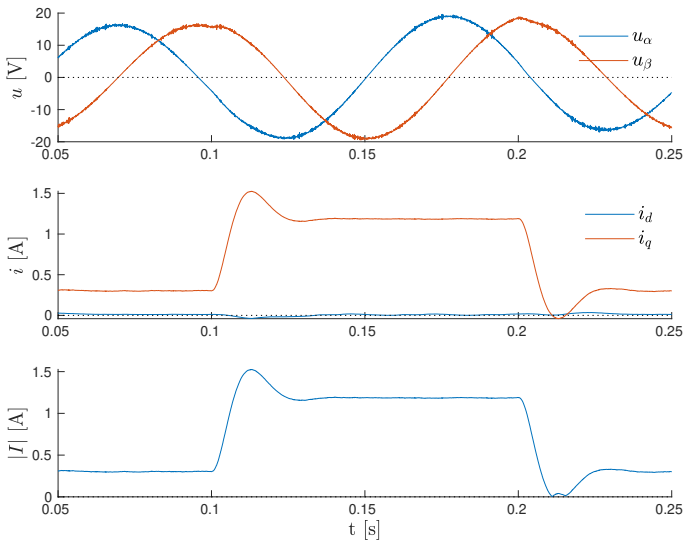

Figure 8. $\alpha\beta$ axis control voltages, dq axis current value, and current modulus during torque acting.

The proposed control algorithms are able to respond quickly to significant disturbances. A fixed error in the controlled speed ω_r appeared. In some cases, where speed is at a standstill, some systematic fixed errors are encountered, and the source is static disturbances like observed rough friction. The proposed solution and presented results can be compared with other works, including [4,10,13,17]. The quality of the obtained estimates and the quality of control are similar, with the same level of estimation errors and control times. The resulting performance, particularly in terms of noise from system state estimation methods, is comparable.

The model considered during the control design phase failed to account for the permanent disturbance, which could potentially explain the outcome. Based on the observed values (e.g., $\hat{T}_l$) from the UKF, it is possible to cancel all these errors, which could be a subject for further research.

4. Conclusions

This paper stands out for its significant contribution in introducing an original sensorless control scheme for permanent magnet drives, emphasizing the utilization of Model Predictive Control (MPC) to attain an exceptionally dynamic performance. Notably, the controller's robust performance is showcased across a spectrum of operating points, demonstrating its effectiveness even under challenging conditions such as zero speed.

A noteworthy result is the application of the dq model for control signal prediction, which engenders a control strategy reminiscent of vector control, as discussed by Vas [2]. This strategic alignment adds a layer of versatility to the proposed control scheme, broadening its applicability in diverse operational scenarios.

The demonstrated advantages of the MPC algorithm in high-dynamic systems underscore its suitability for situations characterized by rapid speed changes. This paper not only presents a successful design of an MPC-based control system incorporating an unscented Kalman filter but also highlights ongoing efforts aimed at further reducing the control errors and refining dynamical behavior. Moreover, there are plans to implement the proposed algorithm in an industrial drive system with constrained computing hardware, emphasizing the practicality and scalability of the proposed approach.

While the discussed topics have garnered considerable attention, there remains ample space for additional research and development in this field. Exploring the integration of predictive control with other established control methods not only holds promise for advancing the current understanding but also opens up avenues for innovative applications and improvements in control strategies for diverse systems. This paper thus serves as a springboard for continued exploration and investigations into the evolving landscape of advanced control methodologies in the realm of sensorless permanent magnet drives.

Funding: This research received no external funding.

Data Availability Statement: Dataset available on request from the author.

Conflicts of Interest: The author declare no conflict of interest.

Abbreviations

The following abbreviations are used in this manuscript:

EKF	Extended Kalman Filter
EMF	Electromagnetic Force
IAE	Integral Absolute Error
ITAE	Integral Time Absolute Error
MPC	Model Predictive Control
PMSM	Permament Magnet Synchronous Motor
QP	Quadratic Programming
UKF	Unscented Kalman Filter

Appendix A

The laboratory setup, motor specifications, and crucial power electronics parameters are detailed in Table A1 below.

Table A1. Laboratory setup parameters.

Parameter	Symbol	Value
Stator phase resistance	R_s	3.55 Ω
Stator inductance (d axis)	L_d	17.16 μH
Stator inductance (q axis)	L_q	17.16 μH
Permanent magnet flux linkage	Ψ_f	2.45 Wb
Number of pole pairs	p	12
Moment of inertia	J	39.5 mkgm^2
Inverter supply voltage	U_{DC}	48
Maximum inverter phase current	I_{max}	25 A
Sampling time	T_s	100 μs

References

1. Pellegrino, G.; Vagati, A.; Guglielmi, P.; Boazzo, B. Performance Comparison Between Surface-Mounted and Interior PM Motor Drives for Electric Vehicle Application. *IEEE Trans. Ind. Electron.* **2012**, *59*, 803–811. [CrossRef]
2. Vas, P. *Vector Control of AC Machines*; Monographs in Electrical and Electronic Engineering; Oxford University Press: Oxford, UK, 1990.
3. Wang, G.; Valla, M.; Solsona, J. Position Sensorless Permanent Magnet Synchronous Machine Drives—A Review. *IEEE Trans. Ind. Electron.* **2020**, *67*, 5830–5842. [CrossRef]
4. Urbanski, K.; Janiszewski, D. Sensorless Control of the Permanent Magnet Synchronous Motor. *Sensors* **2019**, *19*, 3546. [CrossRef] [PubMed]
5. Batzel, T.; Lee, K. Electric propulsion with the sensorless permanent magnet synchronous motor: Model and approach. *IEEE Trans. Energy Convers.* **2005**, *20*, 818–825. [CrossRef]
6. Briz, F.; Degner, M.W. Rotor Position Estimation. *IEEE Ind. Electron. Mag.* **2011**, *5*, 24–36. [CrossRef]
7. Vas, P. *Sensorless Vector and Direct Torque Control*; Monographs in Electrical and Electronic Engineering; Oxford University Press: Oxford, UK, 1998; Number 42.
8. Schroedl, M. An improved position estimator for sensorless controlled permanent magnet synchronous motors. In Proceedings of the 4th European Conference on Power Electronics and Applications–EPE '91, Firenze, Italy, 3–6 September 1991 ; Volume 3, pp. 418–423.
9. Wang, S.; Yang, K.; Chen, K. An Improved Position-Sensorless Control Method at Low Speed for PMSM Based on High-Frequency Signal Injection into a Rotating Reference Frame. *IEEE Access* **2019**, *7*, 86510–86521. [CrossRef]
10. Urbanski, K. Estimation of Back EMF for PMSM at Low Speed Range. *MM Mod. Mach. Sci. J.* **2015**, 564–569. [CrossRef]
11. He, C.; Xu, S.; Yan, B.; Wang, Z.; Wang, M. A Fixed-Point Position Observation Algorithm and System-on-Chip Design Suitable for Sensorless Control of High-Speed Permanent Magnet Synchronous Motor. *Electronics* **2023**, *12*, 3160. [CrossRef]
12. Woldegiorgis, A.T.; Ge, X.; Li, S.; Hassan, M. Extended Sliding Mode Disturbance Observer-Based Sensorless Control of IPMSM for Medium and High-Speed Range Considering Railway Application. *IEEE Access* **2019**, *7*, 175302–175312. [CrossRef]
13. Ma, Z.; Zhang, X. FPGA Implementation of Sensorless Sliding Mode Observer with a Novel Rotation Direction Detection for PMSM Drives. *IEEE Access* **2018**, *6*, 55528–55536. [CrossRef]
14. Kalman, R.E. A New Approach to Linear Filtering and Prediction Problems. *Trans. ASME–J. Basic Eng.* **1960**, *82*, 35–45. [CrossRef]
15. Taheri, A.; Ren, H.; Holakooie, M.H. Sensorless Loss Model Control of the Six-Phase Induction Motor in All Speed Range by Extended Kalman Filter. *IEEE Access* **2020**, *8*, 118741–118750. [CrossRef]
16. Wang, Y.; Yu, H.; Che, Z.; Wang, Y.; Zeng, C. Extended State Observer-Based Predictive Speed Control for Permanent Magnet Linear Synchronous Motor. *Processes* **2019**, *7*, 618. [CrossRef]
17. Dilys, J.; Stankevič, V.; Łuksza, K. Implementation of Extended Kalman Filter with Optimized Execution Time for Sensorless Control of a PMSM Using ARM Cortex-M3 Microcontroller. *Energies* **2021**, *14*, 3491. [CrossRef]
18. Julier, S.J. The scaled unscented transformation. In Proceedings of the 2002 American Control Conference (IEEE Cat. No.CH37301), Anchorage, AK, USA, 8–10 May 2002; Volume 6, pp. 4555–4559. [CrossRef]
19. Julier, S.J.; Uhlmann, J.K. Unscented filtering and nonlinear estimation. *Proc. IEEE* **2004**, *92*, 401–422. [CrossRef]
20. Yin, L.; Deng, Z.; Huo, B.; Xia, Y.; Li, C. Robust Derivative Unscented Kalman Filter Under Non-Gaussian Noise. *IEEE Access* **2018**, *6*, 33129–33136. [CrossRef]
21. Rosafalco, L.; Eftekhar Azam, S.; Manzoni, A.; Corigliano, A.; Mariani, S. Unscented Kalman Filter Empowered by Bayesian Model Evidence for System Identification in Structural Dynamics. *Comput. Sci. Math. Forum* **2022**, *2*, 3. [CrossRef]

22. Janiszewski, D. Load torque estimation in sensorless PMSM drive using Unscented Kalman Filter. In Proceedings of the 2011 IEEE International Symposium on Industrial Electronics, Gdansk, Poland, 27–30 June 2011; pp. 643–648. [CrossRef]
23. Gustafsson, F.; Hendeby, G. Some Relations Between Extended and Unscented Kalman Filters. *Signal Process. IEEE Trans.* **2012**, *60*, 545–555. [CrossRef]
24. Hendeby, G.; Karlsson, R.; Gustafsson, F. Particle Filtering : The Need for Speed. *EURASIP J. Adv. Signal Process.* **2010**, *2010*, 181403. [CrossRef]
25. Grüne, L.; Pannek, J. Nonlinear Model Predictive Control. In *Nonlinear Model Predictive Control: Theory and Algorithms*; Springer: London, UK, 2011; pp. 43–66. [CrossRef]
26. Corriou, J.P. *Process Control: Theory and Applications*; Springer: London, UK, 2004; Chapter Model Predictive Control; pp. 575–615. [CrossRef]
27. García, C.E.; Prett, D.M.; Morari, M. Model predictive control: Theory and practice–A survey. *Automatica* **1989**, *25*, 335–348. [CrossRef]
28. Comarella, B.V.; Carletti, D.; Yahyaoui, I.; Encarnação, L.F. Theoretical and Experimental Comparative Analysis of Finite Control Set Model Predictive Control Strategies. *Electronics* **2023**, *12*, 1482. [CrossRef]
29. Morel, F.; Lin-Shi, X.; Retif, J.M.; Allard, B.; Buttay, C. A Comparative Study of Predictive Current Control Schemes for a Permanent-Magnet Synchronous Machine Drive. *IEEE Trans. Ind. Electron.* **2009**, *56*, 2715–2728. [CrossRef]
30. Peng, J.; Yao, M. Overview of Predictive Control Technology for Permanent Magnet Synchronous Motor Systems. *Appl. Sci.* **2023**, *13*, 6255. [CrossRef]
31. Zhang, A.; Lin, Z.; Wang, B.; Han, Z. Nonlinear Model Predictive Control of Single-Link Flexible-Joint Robot Using Recurrent Neural Network and Differential Evolution Optimization. *Electronics* **2021**, *10*, 2426. [CrossRef]
32. Cortes, P.; Kazmierkowski, M.P.; Kennel, R.M.; Quevedo, D.E.; Rodriguez, J. Predictive Control in Power Electronics and Drives. *IEEE Trans. Ind. Electron.* **2008**, *55*, 4312–4324. [CrossRef]
33. Rojas, C.A.; Yuz, J.I.; Silva, C.A.; Rodriguez, J. Comments on "Predictive Torque Control of Induction Machines Based on State-Space Models ". *IEEE Trans. Ind. Electron.* **2014**, *61*, 1635–1638. [CrossRef]
34. Cataldo, P.; Jara, W.; Riedemann, J.; Pesce, C.; Andrade, I.; Pena, R. A Predictive Current Control Strategy for a Medium-Voltage Open-End Winding Machine Drive. *Electronics* **2023**, *12*, 1070. [CrossRef]
35. Darba, A.; De Belie, F.; D'haese, P.; Melkebeek, J.A. Improved Dynamic Behavior in BLDC Drives Using Model Predictive Speed and Current Control. *IEEE Trans. Ind. Electron.* **2016**, *63*, 728–740. [CrossRef]
36. Li, J.; Zhang, L.; Niu, Y.; Ren, H. Model predictive control for extended Kalman filter based speed sensorless induction motor drives. In Proceedings of the 2016 IEEE Applied Power Electronics Conference and Exposition (APEC), Long Beach, CA, USA, 20–24 March 2016; pp. 2770–2775. [CrossRef]
37. Soliman, A.I.; Farhan, A.; Abdelrahem, M.; Kennel, R. Enhanced Sensorless Model Predictive Control of Induction Motor Based on Extended Kalman Filter. In Proceedings of the 2019 IEEE Conference on Power Electronics and Renewable Energy (CPERE), Aswan, Egypt, 23–25 October 2019; pp. 309–313. [CrossRef]
38. Janiszewski, D. Extended Kalman Filter Based Speed Sensorless PMSM Control with Load Reconstruction. In Proceedings of the IECON 2006-32nd Annual Conference IEEE Industrial Electronics, Paris, France, 6–10 November 2006; pp. 1465–1468. [CrossRef]
39. Janiszewski, D. Disturbance estimation for sensorless PMSM drive with Unscented Kalman Filter. In Proceedings of the 12th IEEE Int Advanced Motion Control (AMC) Workshop, Sarajevo, Bosnia and Herzegovina, 25–27 March 2012; pp. 1–7. [CrossRef]
40. Pillay, P.; Krishnan, R. Modeling, simulation, and analysis of permanent-magnet motor drives. I. The permanent-magnet synchronous motor drive. *IEEE Trans. Ind. Appl.* **1989**, *25*, 265–273. [CrossRef]
41. Wan, E.A.; Van Der Merwe, R.; Nelson, A.T. Dual Estimation and the Unscented Transformation. In Proceedings of the 12th International Conference on Neural Information Processing Systems, Cambridge, MA, USA, 29 November–4 December 1999; pp. 666–672.
42. Goodwin, G.C.; Sin, K.S. *Adaptive Filtering Prediction and Control*; Dover Books on Electrical Engineering; Dover Publications: Mineola, NY, USA, 2009.
43. Onat, A. A Novel and Computationally Efficient Joint Unscented Kalman Filtering Scheme for Parameter Estimation of a Class of Nonlinear Systems. *IEEE Access* **2019**, *7*, 31634–31655. [CrossRef]
44. Wan, E.A.; Van Der Merwe, R. The unscented Kalman filter for nonlinear estimation. In Proceedings of the IEEE 2000 Adaptive Systems for Signal Processing, Communications, and Control Symposium (Cat. No.00EX373), Lake Louise, AB, Canada, 4 October 2000; pp. 153–158. [CrossRef]
45. Gould, N.; Toint, P.L. Preprocessing for quadratic programming. *Math. Program.* **2004**, *100*, 95–132. [CrossRef]
46. Bartlett, R.; Wachter, A.; Biegler, L. Active set vs. interior point strategies for model predictive control. In Proceedings of the 2000 American Control Conference, ACC (IEEE Cat. No.00CH36334), Chicago, IL, USA, 28–30 June 2000; Volume 6, pp. 4229–4233. [CrossRef]

47. Janiszewski, D. EKF estimation of mechanical quantities for drive with PM Synchronous Motor. In Proceedings of the International Conference on Power Electronics and Intelligent Control for Energy Conservation (PELINCEC 2005), Warszawa, Poland, 16–19 October 2005; p. 2.
48. Kozlowski, K.; Pazderski, D.; Krysiak, B.; Jedwabny, T.; Piasek, J.; Kozlowski, S.; Brock, S.; Janiszewski, D.; Nowopolski, K. High Precision Automated Astronomical Mount. In *Proceedings of the Automation 2019*; Szewczyk, R., Zieliński, C., Kaliczyńska, M., Eds.; Springer: Cham, Switzerland, 2020; pp. 299–315. [CrossRef]